Electrothermal simulation of a defect in a solar cell

O. Breitenstein[a] and J. P. Rakotoniaina[b]
Max-Planck-Institute of Microstructure Physics, Weinberg 2, D-06120 Halle, Germany

(Received 5 November 2004; accepted 10 January 2005; published online 23 March 2005)

A local electrothermal simulation of a model solar cell is presented. A rigorous discussion of the heat dissipation mechanisms in a solar cell is performed, showing that the total dissipated heat splits into heating terms (thermalization, recombination, and Joule heat) and different Peltier cooling terms. Such simulations are important for interpreting lock-in thermography images of real solar cells. The simulated model cell consists of a circular noncontacted region surrounded by a grid line and a nonlinear edge shunt. Based on this simulation, a special lock-in thermography operation mode is proposed, which enables noncontacted regions in real solar cells to be imaged. Experimental results confirm the theoretical predictions. © *2005 American Institute of Physics*.
[DOI: 10.1063/1.1866474]

I. INTRODUCTION

Lock-in thermography (LIT) is a technique for electronic device testing,[1] in which one images local heat sources in microelectronic devices and the lateral homogeneity of the dark current flow in solar cells.[2] Recently, special LIT techniques have been proposed, working under light irradiation of a solar cell, which enable shunt investigations in noncontacted cells to be performed and also inhomogeneities of the minority carrier lifetime in the material to be imaged.[3–5] In particular, Isenberg and Warta[3,4] have described how high lateral current-density regions, leading to series resistance losses, can be imaged by illuminated LIT under short circuit conditions. However, until now no theoretically justified thermal technique was available to image high series resistance regions in a solar cell. Note that a solar cell is a current-delivering device, which has to be connected low ohmically to an electric load. This connection is provided by a network of fine metallic grid lines and two larger bus bars, which are in ohmic contact to the top emitter layer of the cell. If in certain regions this ohmic contact shows too high a resistance, this region is insufficiently coupled to the load, which leads to losses of the efficiency of the cell. Previous techniques to image such high series resistance regions are "Corescan" (COntact REsistance SCANning[6]) and "CELLO" (solar CELl LOcal characterization[7]). However, Corescan slightly "scratches" at the surface, hence it is not strictly nondestructive to the cells, and CELLO suffers from long measurement times in the order of hours.

The key for a detailed understanding of thermal measurements on solar cells is a realistic simulation of all thermal processes in the device. Such local electrothermal modelings are widespread for microelectronic or power devices, but have not been applied to solar cells yet. The quantitative interpretation of dark LIT results has been made hitherto by assuming that there is only heating action present.[2] However, it was mentioned by Kaes *et al.*[5] that Peltier cooling may play a considerable role as well. The heat dissipation mechanisms in an illuminated solar cell have been discussed both by Isenberg and Warta[3,4] and Kaes *et al.*,[5] but there no local device simulation was performed, and especially the influence of the Peltier cooling at the *p-n* junction has not been considered explicitly. In this contribution we will present a rigorous discussion of the heat dissipation mechanisms in a solar cell. Based on this discussion, a two-dimensional electrothermal simulation is performed of a model solar cell, which shows the typical behavior of a noncontacted region in a real solar cell, including the influence of shunts.

II. PHYSICAL BASICS

A. Thermal simulation

In our simulation we will neglect hole injection from the base into the emitter, holes photogenerated in the emitter, finite contact resistances, radiative recombination, ohmic shunting, and Joule heating in the base; corresponding terms may simply be added. Figure 1 schematically shows the elementary heat dissipation mechanisms we will consider in the illuminated solar cell. These are recombination in the depletion region (P_{dr}), recombination of injected electrons in the base region or at the back surface (P_{base}), thermalization heat of photogenerated electrons (P_{th}), Peltier heating or cooling at the metal-emitter contact (P_{ME}), Peltier cooling for carrier injection at the *p-n* junction ($P_{p\text{-}n-}$), thermalization heat of photogenerated electrons crossing the barrier ($P_{p\text{-}n+}$) [which may also be called Peltier heating, since it is

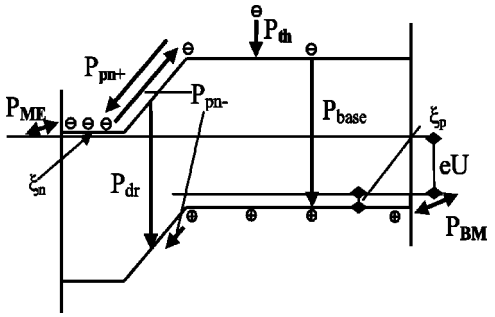

FIG. 1. The dominant heat dissipation mechanisms in a solar cell.

[a]FAX: +49-345-5511223; electronic mail: breiten@mpi-halle.mpg.de
[b]FAX: +49-345-5511223; electronic mail: pati@mpi-halle.mpg.de

the inverse process of $(P_{p\text{-}n\text{-}})$], Peltier heating or cooling at the base-metal contact (P_{BM}), and Joule heating due to horizontal current flow in the emitter (P_J, not indicated in Fig. 1). In a real device all these contributions may be position dependent, depending on the layout of the cell, the local defect distribution, and the working point of the cell. In Fig. 1 also ξ_n and ξ_p are indicated, which are the differences of the Fermi levels to the corresponding band edges in the *n* and the *p* material, respectively. We will also assume in our simulation that all photogenerated carriers contribute to the photocurrent density J_{ph}. This is a good approximation for monochromatic illumination of 880-nm wavelength, having a penetration depth well below the diffusion length, which should be used for the proposed measurements. If white light should be used for illumination, a realistic quantitative evaluation has to include also the recombination of photogenerated carriers in the base and at the back contact. The Peltier effect is treated here in nondegeneracy approximation, hence the amount of thermalization heat or cooling power, respectively, generated by a charge carrier crossing an energy barrier, is given by the corresponding barrier height. Under these conditions, for a local bias of $U(x,y)$, the amounts of the different power densities are the following:

$$P_{\mathrm{dr}}(x,y) = \frac{J_{\mathrm{dr}}(x,y)}{e} E_g, \tag{1}$$

$$P_{\mathrm{base}}(x,y) = \frac{J_{\mathrm{diff}}(x,y)}{e} E_g, \tag{2}$$

$$P_{\mathrm{th}} = \frac{J_{\mathrm{ph}}}{e}(h\nu - E_g), \tag{3}$$

$$P_{\mathrm{ME}}(x,y) = \frac{-J_{\mathrm{ME}}(x,y)}{e}\xi_n, \tag{4}$$

$$P_{p\text{-}n\text{-}}(x,y) = \frac{-[J_{\mathrm{diff}}(x,y) + J_{\mathrm{dr}}(x,y)]}{e} \times [E_g - \xi_n - \xi_p - eU(x,y)], \tag{5}$$

$$P_{p\text{-}n+}(x,y) = \frac{J_{\mathrm{ph}}(x,y)}{e}[E_g - \xi_n - \xi_p - eU(x,y)], \tag{6}$$

$$P_{\mathrm{BM}}(x,y) = \frac{-J_{\mathrm{BM}}(x,y)}{e}\xi_p, \tag{7}$$

$$P_J(x,y) = \rho_s J_{\mathrm{lat}}^2(x,y), \tag{8}$$

with

$$J_{\mathrm{diff}}(x,y) = J_0(x,y)\exp\left[\frac{eU(x,y)}{kT}\right] \tag{9}$$

[$J_{\mathrm{dr}}(x,y)$ = depletion region recombination current density, $J_{\mathrm{diff}}(x,y)$ = diffusion (injection) current density, $J_0(x,y)$ = saturation current density, $J_{\mathrm{ph}}(x,y)$ = photocurrent density, e = electron charge, E_g = band-gap energy, $h\nu$ = photon energy, $J_{\mathrm{ME}}(x,y)$ = emitter contact current density, $J_{\mathrm{BM}}(x,y)$ = base contact current density, ξ_n = difference between Fermi level in *n* material to the conduction-band edge, ξ_p = difference between Fermi level in *p* material to the valence-band edge, $U(x,y)$ = local forward bias, ρ_s = emitter sheet resistance, and J_{lat} = lateral emitter current density (A/m)]. Note that in (5) both the diffusion current and the depletion region recombination current appear, since for the latter the sum of the neccessary energy gain of electrons and holes is the *p*-*n* barrier height as well. Note also that, for a strictly vertical current flow in a laterally homogeneous device ($J_{\mathrm{ME}}=J_{\mathrm{BM}}=J_{\mathrm{diff}}+J_{\mathrm{dr}}-J_{\mathrm{ph}}$), the sum of (1)–(7) is

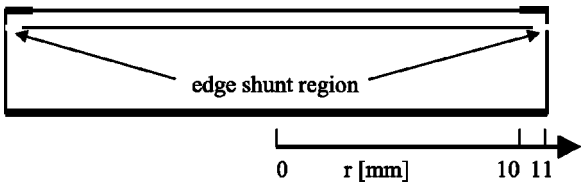

FIG. 2. Cross section of the circular model solar cell (not to scale).

$$P_{\mathrm{tot}} = (J_{\mathrm{dr}} + J_{\mathrm{diff}})U + J_{\mathrm{ph}}\frac{h\nu}{e} - J_{\mathrm{ph}}U. \tag{10}$$

Hence, for strictly vertical current flow in a thermally thin device all Peltier contributions at the contacts are not appearing explicitly anymore in the sum of (1)–(7), and the total dissipated power equals the power dissipated in the dark plus the energy of the irradiated photons minus the power generated by the photocurrent, as expected from the law of energy conservation. However, as soon as nonvertical current flow is considered (e.g., for shunt investigations under illumination[5]), all Peltier contributions have to be taken into account explicitly.

B. Electronic simulation

Our model solar cell consists of a circular homogeneous silicon cell of 22-mm diameter with a 50-Ω/sq emitter on top, a 1-mm-wide ring-shaped emitter contact at the edge, and a full area base metallization (see Fig. 2). Thus, the circular inner part mimics a noncontacted region of a real solar cell. In a 0.5-mm-wide outer ring a depletion region recombination current is assumed to exist, which mimics the usual nonlinear edge shunt region known from most solar cells,[2]

$$J_{\mathrm{dr}} = J_{02}\exp\left(\frac{eU}{2kT}\right). \tag{11}$$

In polar coordinates, the radial current flow in the emitter is $I_{\mathrm{lat}}(r) = 2\pi r J_{\mathrm{lat}}(r)$, and the noncontacted region can be described by the following equations:

$$\frac{dI_{\mathrm{lat}}(r)}{dr} = 2\pi r J_{\mathrm{diff}}(r), \tag{12}$$

$$\frac{dU(r)}{dr} = \frac{\rho_s}{2\pi r} I_{\mathrm{lat}}(r). \tag{13}$$

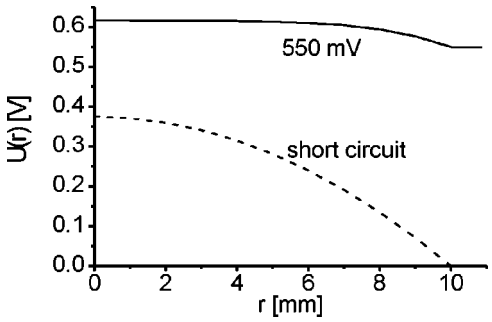

FIG. 3. Emitter potential profiles for two different load conditions (dashed: short circuit at rim; solid: 550 mV at rim).

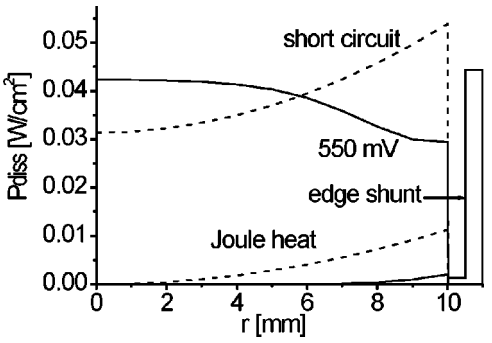

FIG. 4. Dissipated power-density profiles for two different load conditions (dashed: short circuit at rim; solid: 550 mV at rim).

III. RESULTS

A. Simulations

The system of differential Eqs. (12) and (13) has been solved numerically using MATHCAD[8] for the boundary conditions $I_{\mathrm{lat}}(0)=0$ and $U(10\ \mathrm{mm})=0.55$ V (maximum power point of a comparable cell with no series resistance) and 0 V (short circuit), respectively, assuming values of $J_0=1.5\times10^{-12}\mathrm{A/cm^2}$ and $J_{\mathrm{ph}}=30\ \mathrm{mA/cm^2}$. The resulting emitter potential profiles $U(r)$ are shown in Fig. 3. As expected, the potential is always largest in the center of the noncontacted region at $r=0$. From the solution of (12) and (13) for different values of $U(10\ \mathrm{mm})$ it has been found that the maximum power point of this model cell is at 0.43 V, and that its efficiency is only 2/3 of that of a similar cell without any series resistance losses.

Based on these potential distributions, a thermal simulation of the radial dissipated power-density profiles of the model solar cell based on Eqs. (1)–(9) and (11) has been performed. It is assumed here that the sample is thermally thin, hence that all power contributions simply add up, and that the thermalization heat P_{th}, the photocurrent density J_{ph}, and the saturation current density J_0 are distributed homogeneously. Only vertical current flow is assumed in the base, hence $J_{\mathrm{MB}}(x,y)=J_{\mathrm{diff}}(x,y)+J_{\mathrm{dr}}(x,y)-J_{\mathrm{ph}}(x,y)$ holds. Regarding the Peltier effect at the emitter contact, the following estimation was made: the diffusion voltage of the *p-n* junction, which can be measured by evaluating the capacitance–voltage characteristic, should be $V_d=E_g-\xi_n-\xi_p$. For a typical solar cell $V_d=0.97$ eV has been measured by us, leading for $E_g=1.12$ eV to $\xi_n+\xi_p=0.15$ eV. This is already in the order of ξ_p expected for a doping concentration of the base of $10^{16}\ \mathrm{cm^{-3}}$. Therefore, in the following the Peltier effect at the metal-emitter contact (4), for which the degeneracy approximation would not hold anyway, will be neglected here ($\xi_n\approx0$). This is supported by the high doping concentration of the emitter and also by the fact that until now lock-in thermography investigations have given no evidence of any Peltier cooling at grid lines.[2] Hence, in our case the thermal simulations may be performed by using only (8)–(10) instead of using (1)–(9). A homogeneous thermalization heat of 0.3 eV/photon (880-nm light, $h\nu=1.4$ eV) is assumed. At the ring-shaped emitter contact, the light is assumed to be reflected, hence J_{ph} is assumed to be zero there (shading effect). A value of $J_{02}=2\times10^{-6}\mathrm{A/cm^2}$ has been assumed for describing the edge shunt according to (11). Figure 4 shows the results of this modeling for the two load conditions. The Joule heat contribution (8) is separately displayed at the bottom of the graph. We see that at 0.55 V applied at the rim (solid line) the dissipated power is largest in the center and reduces towards the rim, but under short circuit at the rim (dashed line) it is smallest in the center and increases towards the rim. This different radial tendency is not only due to the different Joule contributions, but can easily be understood if the voltage-dependent power dissipation density due to the vertical current is considered by summing up (1)–(8) for constant values of U (which would correspond to a ring-shaped region in our model cell), which equals (10). Figure 5 shows that this dissipated power has a minimum close to 0.55 V, as expected, since this is the maximum power point of the cell without any series resistance losses. If our model solar cell is biased to 0.55 V at the rim region, the potential of its inner part is above that of the minimum in Fig. 5, but if the rim is at short circuit, the inner part is at a bias below this minimum, as Fig. 3 shows. Therefore, the radial tendency of the thermal response is opposite in both cases. The depletion region recombination heat of the edge shunt is present only at 0.55 V, but not at short circuit applied at the rim.

For detecting noncontacted regions, it is most useful to display the difference between the thermal response measured at mpp and that at short circuit. With lock-in thermography this difference can be obtained most easily by keeping the illumination intensity constant and pulsing the load of the cell. The dashed line in Fig. 6 shows the profile of $P_{\mathrm{mpp}}(r)-P_{\mathrm{sc}}(r)$ from the data of Fig. 4. We propose to call this

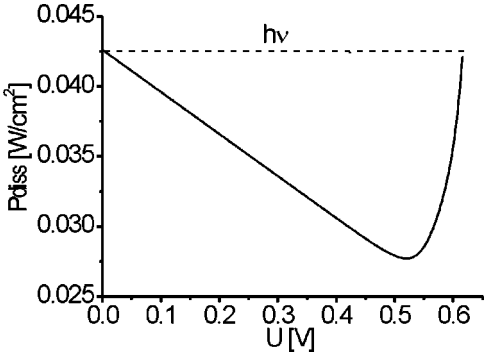

FIG. 5. Dissipated power density as a function of the emitter potential U.

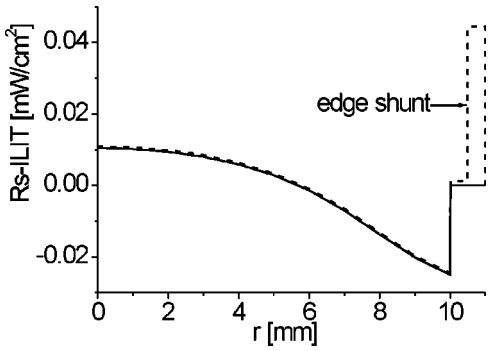

FIG. 6. "R_s-ILIT" signal uncorrected (dashed line) and shunt corrected (solid line).

difference signal "R_s-ILIT" signal (R_s = series resistance, ILIT = illuminated lock-in thermography). This signal is positive in the center of the noncontacted region and becomes negative in well-contacted regions ($r = 10$ mm). Hence, for displaying the R_s-ILIT signal, the −90° LIT signal has to be used instead of the more usual amplitude signal, since the latter is always positive. Note that the edge shunt signal at the rim is still present in this signal. Hence, local shunts could be misinterpreted in the R_s-ILIT signal as high-resistive regions. To avoid this, we propose to subtract the independently measured shunt signal from the R_s-ILIT signal. The shunt signal is a LIT signal measured in the dark at the maximum power point, which may be called "mpp-DLIT" signal (DLIT = dark lock-in thermography). Thus, the shunt-corrected signal, which is optimum for imaging high-resisitivity (noncontacted) regions in solar cells is

$$R_s\text{-ILIT}^{\text{corr}} = R_s\text{-ILIT} - \text{mpp-DLIT}. \tag{14}$$

Also this signal profile is shown for our model cell as a solid line in Fig. 6. Indeed, in this signal the edge shunt contribution is completely canceled.

B. Experimental verification

The validity of our simulations will be proven by introducing various measured LIT results in Fig. 7, which are obtained on a 125×125 mm^2 sized monocrystalline solar cell. This cell was deliberately processed to contain a noncontacted region in the left part of the cell.[9] The measurement took about 1/2 h. All thermal signals visible in Fig. 7 are in the low millikelvin range, bright regions correspond to positive signal. The two horizontal stripes visible in Figs. 7(b) and 7(c) are due to the metallic contact leads to the cell. The DLIT image taken at mpp (a) shows some edge recombination and some local edge shunts as bright spots at the upper edge, which physically correspond to the "edge shunt region" at the outer rim of our simulation. Note that this image (a) shows no indication of a noncontacted region. The uncorrected R_s-ILIT signal (b) clearly shows this region at the left as a bright region. In contrast with our simulation, this region is not circular shaped but vertically extended, but the bright signal appears as expected. This uncorrected image (b) also shows the local edge shunts as additional bright spots. Only the shunt-corrected R_s-ILIT signal (c) shows the noncontacted region as the only dominant signal.

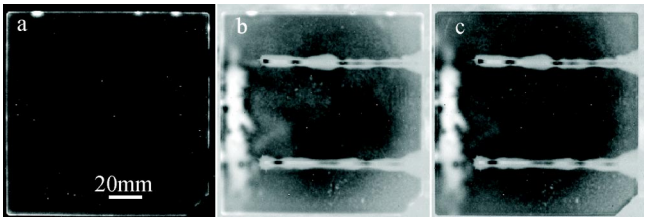

FIG. 7. (a) Shunt image (mpp, no illumination), (b) uncorrected R_s-ILIT image, and (c) shunt-corrected R_s-ILIT image, all experimentally measured at a solar cell.

IV. DISCUSSION

In this contribution a rigorous discussion of the heat dissipation mechanisms in a solar cell was performed, showing that the total heat dissipation splits into heating terms (thermalization, recombination, and Joule heat) and different Peltier cooling terms. We have performed a local electrothermal simulation of a model solar cell, which mimics a high-resistance defect in a real solar cell. Based on these simulations, a special resistance-imaging lock-in thermography technique was introduced. Though this technique does not allow to measure local series resistances quantitatively yet, it should be useful in solar cell technology and research for detecting regions of high contact resistance, since it is nondestructive, and the measurement can be performed within a reasonable measurement time. In the simple model solar cell simulated in this contribution, the different types of Peltier effects do not have to be considered explicitly, since only vertical current flow is assumed and the Peltier effect at the emitter contact is neglected. However, as soon as also horizontal current flow in the base is considered, as it is the case, e.g., for photocurrent-induced shunt imaging or generally for describing strongly localized shunts, the detailed set of equations containing the Peltier terms has to be used for a correct local thermal modeling. In the presence of strongly recombining local defects, also our assumption of a homogeneous distribution of J_0 and J_{ph} is not valid anymore. Furthermore, for microscopic modeling also the different depths of the various heat/cooling sources in the cell have to be be taken into account. Also in these cases eqs. (1)–(9) and a recombination term corresponding to (11) provide the basis for a detailed local thermal analysis of defects in solar cells.

This work was supported by the German BMBF under Contract No. 0329846 D (ASIS). We wish to thank A.S.H. van der Heide (ECN Petten) for delivering the solar cell used for this investigation and for stimulating discussions, and U. Gösele (Halle), J. Isenberg and W. Warta (ISE Freiburg), and M. Kaes and G. Hahn (Univ. Konstanz) for stimulating discussions.

[1]Thermosensorik GmbH Erlangen/Germany, www.thermosensorik.com
[2]O. Breitenstein and M. Langenkamp, *Lock-in Thermography-Basics and Use for Functional Diagnostics of Electronic Components* (Springer, Berlin, 2003).
[3]J. Isenberg and W. Warta, J. Appl. Phys. **95**, 5200 (2004).

[4]J. Isenberg and W. Warta, Prog. Photovoltaics **12**, 339 (2004).
[5]M. Kaes, S. Seren, T. Pernau, and G. Hahn, Prog. Photovoltaics **12**, 355 (2004).
[6]A. S. H. van der Heide, J. H. Bultman, J. Hoornstra, and A. Schönecker, Sol. Energy Mater. Sol. Cells **74**, 43 (2002).
[7]J. Carstensen, G. Popkirov, J. Bahr, and H. Föll, Sol. Energy Mater. Sol. Cells **76**, 599 (2003).
[8]www.mathcad.com
[9]J. Hoornstra, A. S. H. van der Heide, A. W. Weeber, and F. Granek, *Proceedings of the 19th European Photovoltaic Solar Energy Conference, Paris, 7–11 June 2004*, edited by W. Hoffmann, J.-L. Bal, H. Ossenbrink, W. Palz, and P. Helm (WIP, Munich, 2004) pp. 1044–1047.